## Title

Mesenchymal gene program–expressing ovarian cancer spheroids exhibit enhanced mesothelial clearance



## Journal

Journal of Clinical Investigation, 124(6)

## ISSN

0021-9738

## Authors

Davidowitz, Rachel A
Selfors, Laura M
Iwanicki, Marcin P
et al.

## Publication Date

2014-06-02

## DOI

10.1172/jci69815

Peer reviewed

# Mesenchymal gene program–expressing ovarian cancer spheroids exhibit enhanced mesothelial clearance

Rachel A. Davidowitz,[1] Laura M. Selfors,[1] Marcin P. Iwanicki,[1] Kevin M. Elias,[2,3] Alison Karst,[2] Huiying Piao,[2] Tan A. Ince,[4] Michael G. Drage,[5] Judy Dering,[6] Gottfried E. Konecny,[6] Ursula Matulonis,[2] Gordon B. Mills,[7] Dennis J. Slamon,[6] Ronny Drapkin,[2,5] and Joan S. Brugge[1]

[1]Department of Cell Biology, Harvard Medical School, Boston, Massachusetts, USA. [2]Dana-Farber Cancer Institute, Department of Medical Oncology, Center for Molecular Oncologic Pathology, Boston, Massachusetts, USA. [3]Brigham and Women's Hospital, Division of Gynecologic Oncology, Department of Obstetrics, Gynecology, and Reproductive Biology, Boston, Massachusetts, USA. [4]Department of Pathology, Interdisciplinary Stem Cell Institute, Braman Family Breast Cancer Institute, and Sylvester Comprehensive Cancer Center, University of Miami Miller School of Medicine, Miami, Florida, USA. [5]Brigham and Women's Hospital, Department of Pathology, Boston, Massachusetts, USA. [6]Division of Hematology-Oncology, David Geffen School of Medicine, UCLA, Los Angeles, California, USA. [7]Department of Bioinformatics and Computational Biology, The University of Texas MD Anderson Cancer Center, Houston, Texas, USA.

**Metastatic dissemination of ovarian tumors involves the invasion of tumor cell clusters into the mesothelial cell lining of peritoneal cavity organs; however, the tumor-specific factors that allow ovarian cancer cells to spread are unclear. We used an in vitro assay that models the initial step of ovarian cancer metastasis, clearance of the mesothelial cell layer, to examine the clearance ability of a large panel of both established and primary ovarian tumor cells. Comparison of the gene and protein expression profiles of clearance-competent and clearance-incompetent cells revealed that mesenchymal genes are enriched in tumor populations that display strong clearance activity, while epithelial genes are enriched in those with weak or undetectable activity. Overexpression of transcription factors SNAI1, TWIST1, and ZEB1, which regulate the epithelial-to-mesenchymal transition (EMT), promoted mesothelial clearance in cell lines with weak activity, while knockdown of the EMT-regulatory transcription factors TWIST1 and ZEB1 attenuated mesothelial clearance in ovarian cancer cell lines with strong activity. These findings provide important insights into the mechanisms associated with metastatic progression of ovarian cancer and suggest that inhibiting pathways that drive mesenchymal programs may suppress tumor cell invasion of peritoneal tissues.**

## Introduction

Ovarian cancer has the highest mortality rate of all gynecological cancers and the fifth highest mortality rate of all cancers in the United States (1). Because early disease is asymptomatic, ovarian cancer is rarely diagnosed until late stages, when the cancer has spread beyond the primary tumor site (2). Ovarian cancer metastasis involves detachment of tumor cells from the primary tumor site and attachment on the surface of other intra-abdominal organs (3, 4), including the omentum, peritoneum, diaphragm, and small bowel mesentery (5). Generally, tumor nodules develop on the surface of the peritoneal organs and undergo extensive expansion, leading to significant clinical complications, including bowel obstruction.

All of the organs within the peritoneal cavity are lined with a continuous monolayer of mesothelial cells (6–8). Electron micrograph studies of ovarian cancer nodules attached to peritoneal cavity organs revealed that mesothelial cells are absent from underneath the attached tumor mass (7–10), suggesting that mesothelial cells can act as a protective barrier against ovarian cancer metastasis and that mesothelial cells are excluded during processes leading to successful tumor cell implantation on peritoneal tissue. This is supported by in vitro evidence that attachment and invasion of ovarian cancer cells into a 3D collagen gel is delayed when the gel is covered with a mesothelial monolayer (11) and that ovarian cancer cells are able to attach more firmly to ECM components compared with either plastic culture dishes or mesothelial cell monolayers (12, 13).

Ovarian cancer cells can attach and spread on multiple ECM proteins associated with the mesothelium and underlying basement membrane, including collagen I, collagen IV, laminin, vitronectin, and fibronectin; α and β integrins, as well as CD44, have been shown to serve as tumor cell receptors for these ligands (9, 12–21). While ovarian cancer cell adhesion and spreading on mesothelial monolayers has been well characterized, there has been much less focus on understanding the mechanisms associated with ovarian cancer cell invasion into and displacement of cells in the mesothelial monolayer. Several groups have examined the ability of single ovarian cancer cells to transverse through a mesothelial monolayer and found that inhibiting VCAM, α4 integrin, β1 integrin, MMP-2, or MMP-9 could decrease the extent of transmesothelial invasion (21–23). In addition, studies from our laboratory have shown that ovarian cancer multicellular spheroids are able to attach to and clear a hole in a mesothelial cell monolayer through an integrin- and force-dependent process involving α5 integrin, talin I, and myosin II. Inhibiting any of these molecules significantly decreases mesothelial clearance ability (24).

In this study, we sought to further understand the mechanisms by which ovarian cancer multicellular spheroids clear the mesothelial monolayer by characterizing the clearance abilities of a panel of 20 established ovarian cancer cell lines and 21 primary ovarian cancer cell samples. Comparison of the gene and protein

**Conflict of interest:** The authors have declared that no conflict of interest exists.
**Citation for this article:** *J Clin Invest.* 2014;124(6):2611–2625. doi:10.1172/JCI69815.

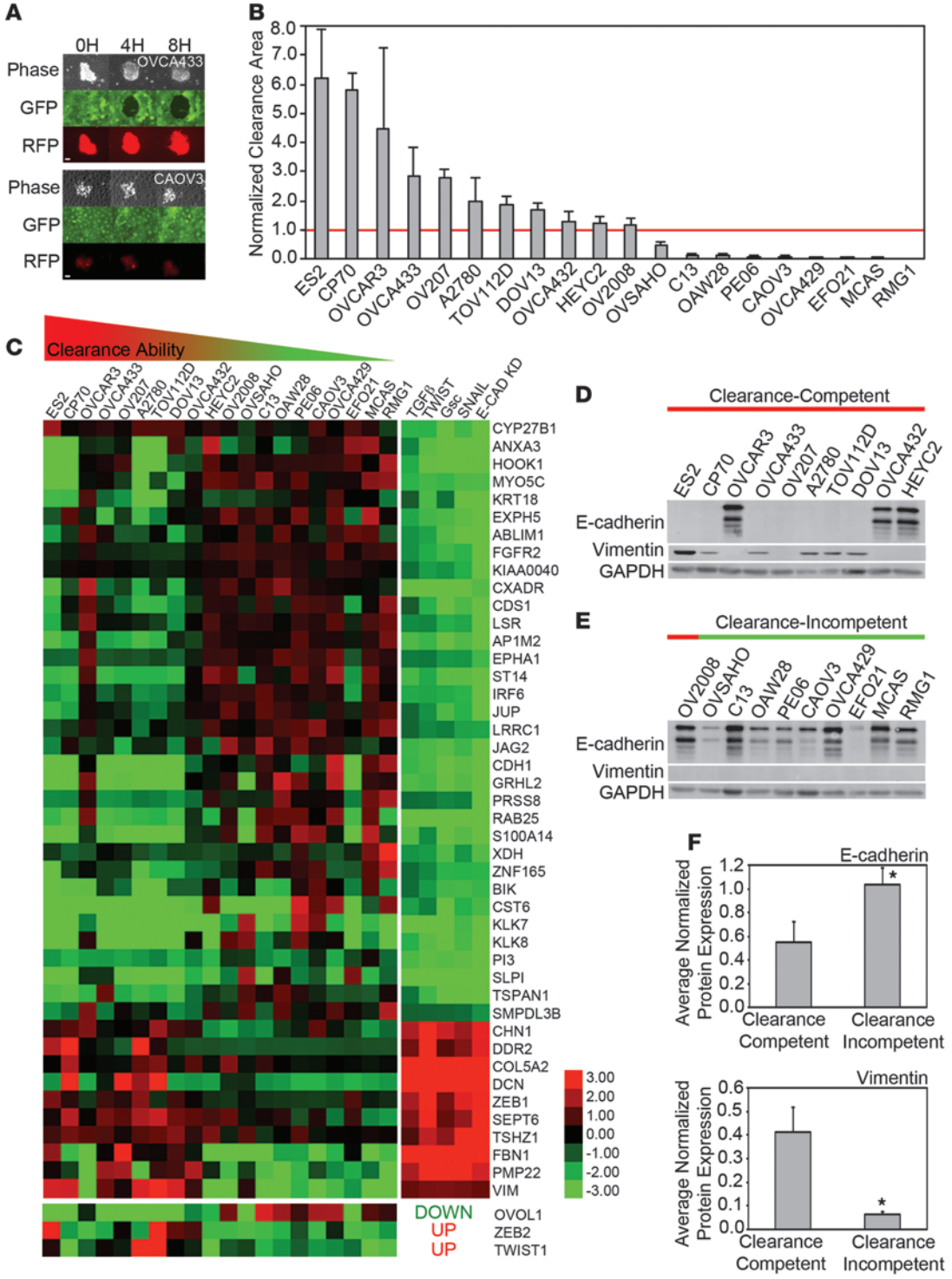

**Figure 1**
Ovarian cancer cell line spheroids display differential clearance ability that correlates with epithelial and mesenchymal marker expression. (**A**) Representative images from mesothelial clearance assays of 2 clearance-competent or clearance-incompetent ovarian cancer cell lines. The extent of clearance of a ZT mesothelial monolayer (green) by OVCA433 or CAOV3 ovarian cancer spheroids (red) was imaged at 0, 4, and 8 hours after coincubation. (**B**) Quantification of clearance by ovarian tumor cell lines. Clearance area was measured in 20 established ovarian cancer cell lines by coculturing preformed multicellular spheroids with ZT mesothelial cell monolayers. After 8 hours of coincubation, the negative space created in the mesothelial monolayer by the ovarian cancer spheroid was measured and divided by the initial size of the ovarian cancer spheroid at time 0 to determine the normalized clearance area. Cell lines with a normalized clearance area >1 were classified as clearance competent and <1 were classified as clearance incompetent. >10 spheroids scored over 2 replicates. (**C**) Analysis of enrichment of mRNAs associated with EMT. Heat map showing mRNA expression of genes associated with the Taube EMT core signature and 3 additional transcription factors that are significantly ($P < 0.05$) differentially expressed in the clearance-competent and clearance-incompetent ovarian tumor cell lines. Ovarian cancer cell line data in the left column and manipulations to HMLE cells from Taube et al. (25) in the right column. Both data sets were $\log_2$ transformed for visualization. (**D**) Western blot analysis of E-cadherin and vimentin expression in the 20 established ovarian cancer cell lines. (**E** and **F**) Average (**E**) E-cadherin or (**F**) vimentin protein expression levels in clearance-competent and clearance-incompetent cell lines measured by densitometry:. Error bars denote SEM. *$P < 0.05$, Student's *t* test. Scale bar: 100 μm.

expression profiles of ovarian cancer spheroids that are competent or incompetent to clear mesothelial monolayers revealed distinct differences in the expression of mesenchymal and epithelial cell markers that correlated with clearance competency. Modulation of mesenchymal transcription factors to promote or inhibit mesenchymal gene expression altered the clearance ability of the tumor cell lines. These studies provide important new insights into the mechanisms involved in mesothelial cell invasion and the pathogenesis of ovarian cancer progression.

## Results

*Differential ability of ovarian cancer spheroids to clear a mesothelial monolayer*. We have shown previously that OVCA433 ovarian cancer multicellular spheroids are able to attach to, intercalate into, and form a hole in a mesothelial cell monolayer, while OVCAR5 ovarian cancer multicellular spheroids are unable to clear the monolayer (24). To explore the differences in gene and protein expression that distinguish clearance-competent ovarian cancer multicellular spheroids from clearance-incompetent spheroids, we first analyzed the ability of preformed multicellular spheroids from 20 different ovarian cancer cell lines to form a hole in GFP-expressing ZT mesothelial monolayers using time-lapse video microscopy (Figure 1A).

After 8 hours of coculture, clearance ability was scored. The cell lines with a normalized clearance area greater than 1 are referred to as clearance competent, while the cell lines with a normalized clearance area less than 1 are referred to as clearance incompetent. Eleven ovarian cancer cell lines (ES2, CP70, OVCAR3, OVCA433, OV207, A2780, TOV112D, DOV13, OVCA432, HEYC2, and OV2008) were able to clear the mesothelial monolayer, 3 (OVSAHO, C13, and OAW28) cleared weakly, and 6 (PE06, CAOV3, OVCA429, EFO21, MCAS, and RMG1) did not clear (Figure 1B, Supplemental Figure 1, and Supplemental Video 1; supplemental material available online with this article; doi:10.1172/JCI69815DS1). These results indicate that there is a continuum of clearance abilities among ovarian cancer spheroids.

*Ovarian cancer spheroid clearance ability correlates with the expression of mesenchymal and epithelial markers*. To explore differences between cell lines with distinct clearance competencies, relative gene expression was measured in the 20 ovarian cancer cell lines using an Agilent Human 44K expression microarray. A total of 1,426 unique genes were identified as distinguishing the clearance-competent cell lines from the clearance-incompetent cell lines ($P < 0.05$, Supplemental Table 1). Enrichment analysis demonstrated that this set was enriched for genes in the GeneGo Pathway Maps: "TGF-β–dependent induction of epithelial-to-mesenchymal transition (EMT) via SMADs" and "regulation of epithelial-to-mesenchymal transition" ($P < 7.37 \times 10^{-5}$ and $P < 5.69 \times 10^{-4}$ respectively, GeneGo). To further validate this pathway enrichment, we analyzed the overlap between our set of differentially expressed genes and an EMT signature consisting of a 159-gene EMT core signature (25) and 6 established EMT transcriptional regulators (*TWIST1*, *TWIST2*, *ZEB2*, *SNAI1*, *SLUG*, *OVOL1*) (26). The genes differentially regulated in clearance-competent cell lines were 2.4-fold enriched for genes in the core EMT signature ($P = 1.94 \times 10^{-8}$, Figure 1C; fold enrichment is defined as the observed frequency divided by the expected frequency). Genes characteristic of a mesenchymal phenotype were enriched in the clearance-competent ovarian cancer cell lines, while genes characteristic of an epithelial phenotype were enriched in the clearance-incompetent cell lines (Figure 1C). Interestingly, OVCA432, HEYC2, and OV2008 cells, which exhibited borderline clearance activity, expressed the weakest mesenchymal signature.

Protein expression of the epithelial marker, E-cadherin, and the mesenchymal marker, vimentin, was confirmed in the ovarian cancer cell lines by Western blot analysis (Figure 1D). Consistent with the microarray data, average E-cadherin protein expression was lower in the clearance-competent cell lines compared with that in the clearance-incompetent cell lines (Figure 1E), whereas, average vimentin protein expression was higher in the clearance-competent cell lines compared with that in the clearance-incompetent cell lines (Figure 1F). The 2 weakest cell lines in the clearance-competent group, OVCA432 and HEYC2, expressed E-cadherin. OVCAR3 cells represent an outlier — both with respect to mRNAs in the EMT signature and E-cadherin protein expression. It is possible that OVCAR3 cells have an additional alteration that could drive intercalation independent of the mesenchymal signature; e.g., these cells carry gene amplifications of *PIK3CA* and *AKT2*, which regulate actin cytoskeletal changes and tumor cell invasion (27). Taken together, these data suggest that clearance-competent cell lines are enriched for mesenchymal markers, while clearance-incompetent cells are enriched for epithelial markers.

*Overexpression of TWIST1, ZEB1, or SNAI1 promotes mesothelial clearance*. To determine whether mesenchymal gene programs functionally regulate mesothelial clearance, we modulated the expression of several EMT transcription factors in the ovarian cancer cell lines and measured the effects on clearance ability. First, we examined whether overexpression of the EMT transcription factors TWIST1, ZEB1, and SNAI1 in a clearance-incompetent cell line (MCAS) could promote clearance ability. TWIST1 and ZEB1 were chosen because their expression was significantly correlated with clearance ability (Figure 1C). SNAI1 was chosen because it is known to be a strong inducer of EMT (28).

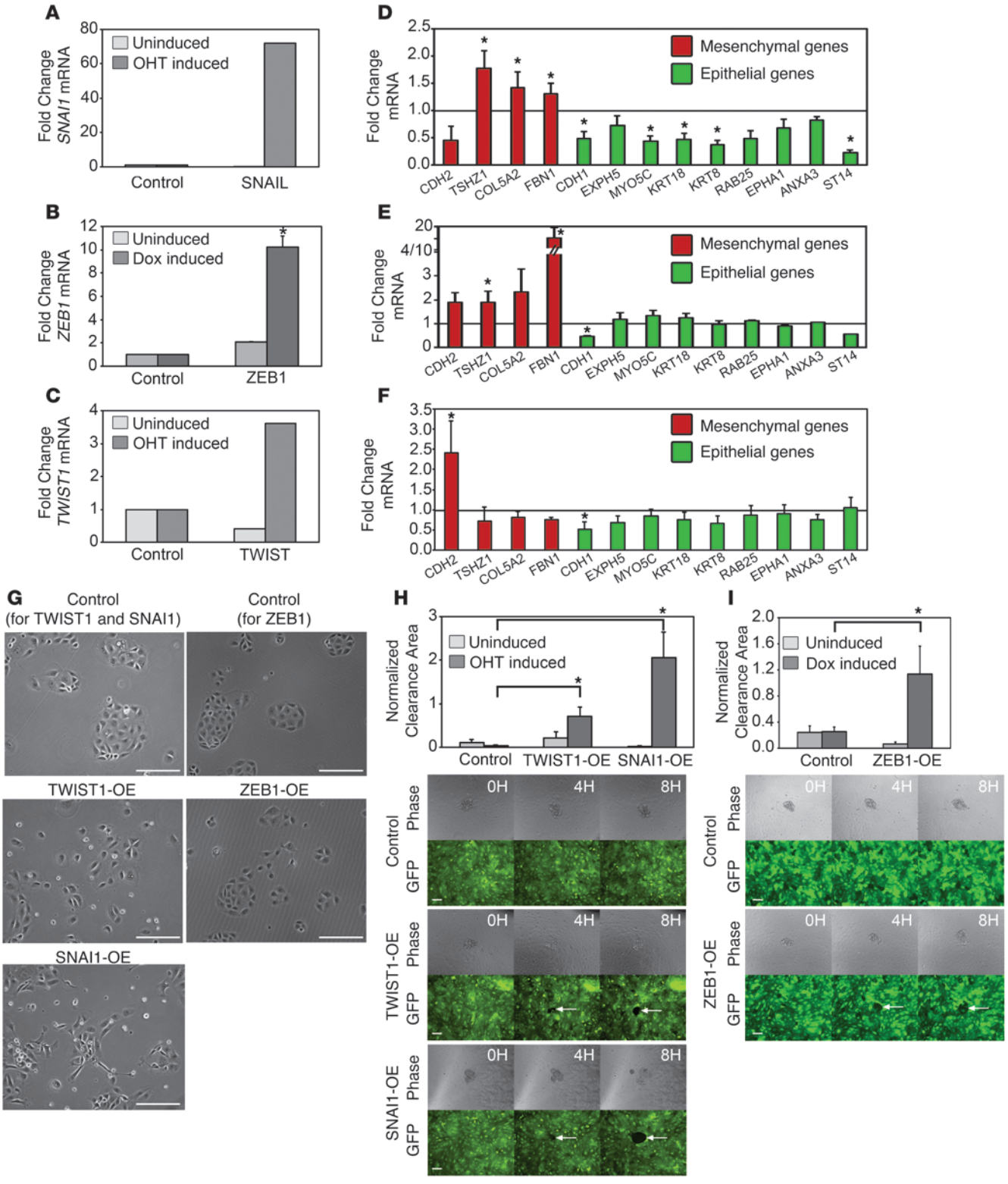

**Figure 2**
Overexpression of EMT transcription factors increases mesothelial clearance ability. (**A**–**C**) qRT-PCR measurements of mRNA levels of (**A**) *SNAI1*, (**B**) *ZEB1*, or (**C**) *TWIST1* in MCAS cells infected with the control WZL-empty vector, WZL-TWIST, or WZL-SNAI1 or MCAS rTTA cells infected with control FUW-LPT2 or FUW-LPT2 ZEB1. TWIST1 and SNAI1 cells were treated with vehicle (uninduced) or 20 nM 4-OHT, while ZEB1 cells treated with vehicle or 1 μg/ml doxycycline. (**D**–**F**) qRT-PCR measurements of mRNA levels of EMT markers in (**D**) TWIST1-, (**E**) ZEB1-, or (**F**) SNAI1-overexpressing cells. Measurements were normalized to *RPLPO* mRNA levels and expressed as fold changes compared to controls. Data are shown as the mean of 3 biological replicates for each condition. Each biological replicate was derived from an average of 3 technical replicates. (**G**) Phase-contrast images of control, TWIST1-, ZEB1-, and SNAI1-overexpressing MCAS cells induced with 20 nM 4-OHT or 1 μg/ml doxycycline for 7 to 14 days. Original magnification, ×10. (**H** and **I**) Normalized average clearance area of ZT mesothelial monolayers 8 hours after coculture with uninduced and 20 nM 4-OHT– or 1 μg/ml doxycycline-induced MCAS spheroids carrying control WZL-empty vector, inducible WZL-TWIST, WZL-SNAIL, control FUW-LPT2, or FUW-LPT2 ZEB1 expression vectors. >20 spheroids averaged per condition. Error bars denote SEM. *$P < 0.05$, Student's *t* test. Scale bar: 100 μm.

We were unable to establish stable lines of MCAS cells overexpressing TWIST1, ZEB1, and SNAI1, most likely because EMT-inducing transcription factors can suppress proliferation when overexpressed in tumor cell lines (29–31); therefore, we inducibly overexpressed these genes in the clearance-incompetent MCAS cell line. Expression was induced for 7 to 14 days by supplementing the growth medium with 20 nM 4-hydroxytamoxifen (4-OHT) (for the TWIST1 and SNAI1 vectors) or 1 μg/ml doxycycline (for the ZEB1 vector) every other day. Induction of SNAI1, ZEB1, or TWIST1 resulted in a 72-fold, 10-fold, or 3.6-fold increase in *SNAI1*, *ZEB1*, or *TWIST1* mRNA, respectively (Figure 2, A–C). The expression of several EMT markers was measured by qPCR in the SNAI1-, ZEB1-, and TWIST1-overexpressing cells. These markers were chosen because they were differentially expressed in the clearance-competent and clearance-incompetent cell lines and are part of the Taube core EMT signature (25) (Figure 1C). SNAI1 overexpression produced the most dramatic change in marker expression, inducing the mesenchymal markers *TSHZ1*, *COL5A*, and *FBN1* and suppressing the epithelial markers E-cadherin, *MYO5C*, *KRT18*, *KRT8*, *ANXA3*, and *ST14* (Figure 2D). ZEB1 overexpression induced the expression of the mesenchymal markers *TSHZ1* and *FBN1* and decreased the expression of E-cadherin, while the expression of other epithelial markers was unchanged (Figure 2E). TWIST1 overexpression induced the expression of the mesenchymal marker N-cadherin and decreased the expression of the epithelial markers E-cadherin and keratin 8 (Figure 2F). Furthermore, phase-contrast imaging of attached cells showed that, while control MCAS cells grouped in small clusters and showed an epithelial-like morphology, TWIST1-, ZEB1-, and SNAI1-overexpressing MCAS cells did not cluster as tightly and were more elongated (Figure 2G). Failure to see a more dramatic switch in the TWIST1- and ZEB1-overexpressing cells (low fold change, only a small number of cells phenotypically different; Figure 2, B, C, and G) could reflect the fact that EMT transcription factor overexpression suppresses proliferation (32), suggesting that only a small number of cells in the population can sustain the EMT switch.

Mesothelial clearance analysis revealed that SNAI1, ZEB1, or TWIST1 overexpression significantly increased the clearance ability of MCAS spheroids compared with that of untransfected and uninduced controls (Figure 2, H and I, and Supplemental Figure 2), and the degree of increase in clearance ability correlated with the strength of epithelial and mesenchymal marker change (Figure 2, D–F). Taken together, these results suggest that the overexpression of EMT transcription factors can increase mesothelial cell clearance ability.

*Knockdown of TWIST1 and ZEB1 reduces mesothelial clearance.* To further evaluate the regulation of clearance by transcription factors that modulate EMT, we decreased the expression of EMT transcription factors in clearance-competent cell lines. Since *TWIST1*, *ZEB1*, and *ZEB2* expression correlated significantly with clearance ability (Figure 1C), we knocked down the expression of TWIST and ZEB transcription factor family members in OVCA433 cells. Knockdown of *ZEB1*, *TWIST1*, *ZEB2*, and *TWIST2* genes with siRNA SMARTpools significantly decreased their respective mRNA expression levels, as measured by qPCR 48 hours after treatment (Figure 3, A–D). Western blot analysis revealed that E-cadherin protein expression was increased in both the TWIST1 and ZEB1 siRNA knockdown cells, while vimentin protein expression was unchanged (Figure 3I). qPCR analysis of other EMT markers revealed that ZEB1 knockdown produced the most dramatic effect, consistent with the strong level of E-cadherin protein expression; *EXPH5*, *KRT18*, *KRT8*, and *ANXA3* mRNAs were significantly increased in the ZEB1 knockdown cells, while *COL5A2* mRNA was significantly decreased (Figure 3E). The effects of TWIST1 and ZEB2 knockdown on EMT marker gene expression were less significant (Figure 3, F and G), and there was no significant marker expression change in TWIST2 knockdown cells (Figure 3H). The weak effects on gene expression, particularly the lack of decrease of vimentin and other mesenchymal markers, could reflect the need for a longer knockdown time to reverse the expression of the mesenchymal gene program (33, 34). Nevertheless, knockdown of TWIST1 and ZEB1 by siRNA in OVCA433 cells enhanced E-cadherin expression and that of several other epithelial markers; therefore, we examined the effects of knockdown on mesothelial clearance.

The TWIST1, TWIST2, and ZEB1 siRNA SMARTpools significantly decreased mesothelial clearance, while the ZEB2 SMARTpools did not (Figure 3J). To validate these findings, we tested the individual siRNAs that comprised the TWIST1, ZEB1, and TWIST2 SMARTpools for clearance inhibition; the reduction in clearance was consistent with the extent of knockdown for TWIST1 and ZEB1 but not TWIST2 (Supplemental Figure 3). Finally, ZEB1 expression was knocked down using shRNA-expressing lentiviral vectors. Three of the four hairpins significantly decreased *ZEB1* mRNA expression (Figure 3K), and the levels of mesothelial clearance correlated with ZEB1 knockdown (Figure 3Q). Western blot analysis revealed that E-cadherin expression inversely correlated with ZEB1 knockdown (Figure 3L). While there was variation in the extent of upregulation or downregulation of EMT markers, overall, the expression of mesenchymal genes was decreased and the expression of epithelial genes was increased in the cells with significant ZEB1 downregulation (Figure 3, M–P). Similar to shRNA-mediated downregulation of ZEB1, stable knockdown of TWIST1 using shRNA lentiviral expression vectors resulted in decreased mesothelial clearance and increased expression of the epithelial markers (Supplemental Figure 4). Moreover, siRNA knockdown of TWIST1 and ZEB1 in a second

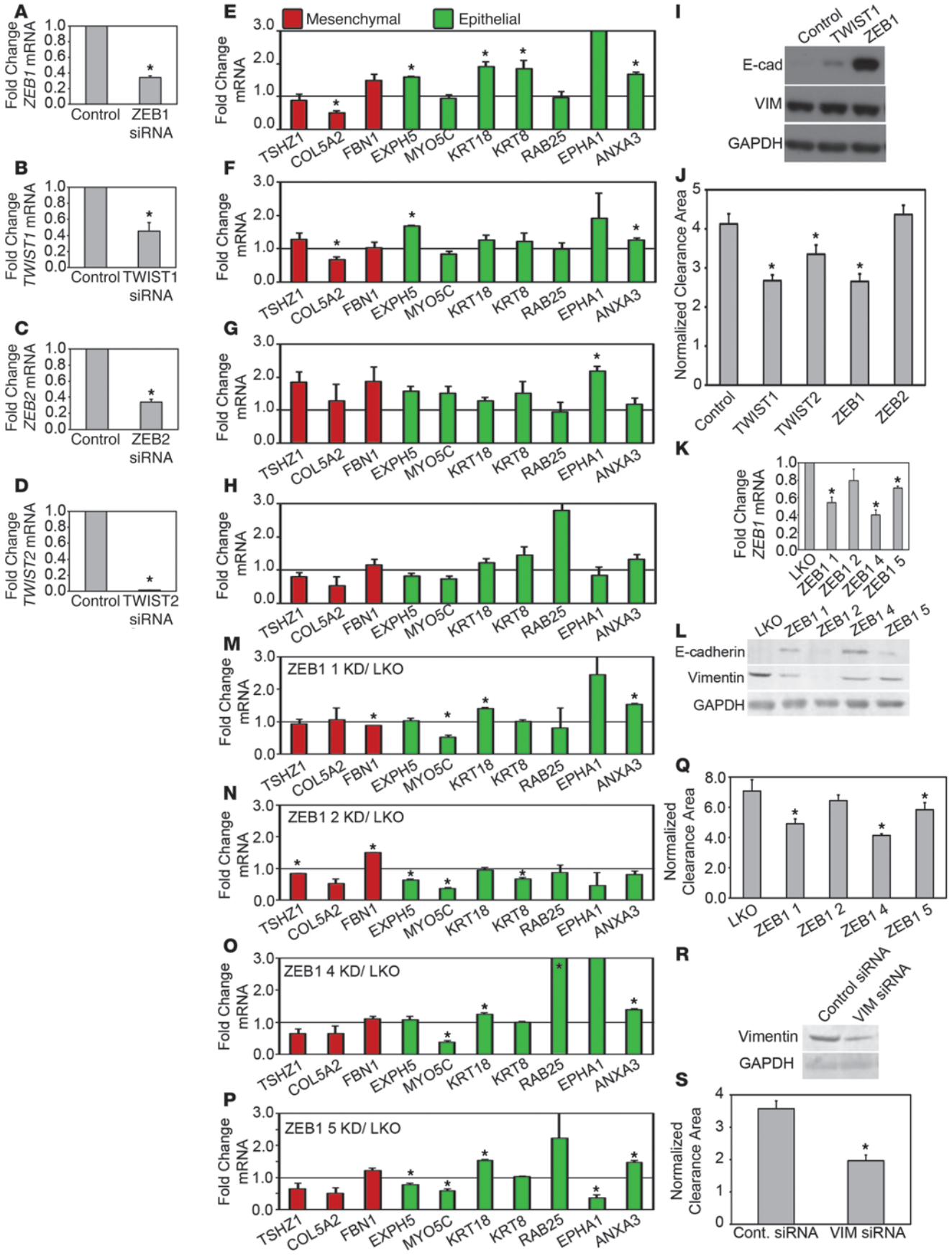

**Figure 3**
Knockdown of EMT transcription factors or vimentin inhibits mesothelial clearance. (**A**–**D**) qRT-PCR measurements of mRNA levels of (**A**) *ZEB1*, (**B**) *TWIST1*, (**C**) *ZEB2*, and (**D**) *TWIST2* in OVCA433 cells transfected with siRNA SMARTpools targeting luciferase (control), ZEB1, TWIST1, ZEB2, or TWIST2. (**E**–**H**) qRT-PCR measurements of mRNA levels of EMT markers in (**E**) ZEB1, (**F**) TWIST1, (**G**) ZEB2, or (**H**) TWIST2 siRNA–treated OVCA433 cells. Measurements were normalized to *RPLPO* mRNA levels and expressed as fold changes compared to controls. Data are shown as the mean of 3 biological replicates for each condition. Each biological replicate was derived from an average of 3 technical replicates. (**I**, **L**, and **R**) Western blot analysis of E-cadherin and vimentin in OVCA433 cells transfected with (**I**) siRNA SMARTpools targeting luciferase, TWIST1, or ZEB1; (**L**) with empty vector control or shRNAs targeting ZEB1; and (**R**) with siRNA SMARTpools targeting luciferase or vimentin. (**J**, **Q**, and **S**) Normalized average clearance area of ZT mesothelial monolayers at 8 hours after coincubation with OVCA433 spheroids transfected with (**J**) luciferase, TWIST1, TWIST2, ZEB1, or ZEB2 siRNA SMARTpools; (**Q**) empty vector control or shRNAs targeting ZEB1; and (**S**) siRNA SMARTpools targeting luciferase or vimentin. >60 positions scored per condition in 3 independent experiments. (**K**) qRT-PCR measurements of mRNA levels of *ZEB1* in OVCA433 cells transfected with empty vector control (LKO) or shRNAs targeting ZEB1. (**M**–**P**) qRT-PCR measurements of mRNA levels of EMT markers in OVCA433 cells transfected with ZEB1 (**M**) shRNA 1, (**N**) shRNA 2, (**O**) shRNA 4, or (**P**) shRNA 5 normalized to control marker expression. Error bars denote SEM. $^*P < 0.05$, Student's *t* test.

cell line, OVCA432, also significantly decreased mesothelial clearance (Supplemental Figure 5). In conclusion, ZEB1 and TWIST1 are required for efficient mesothelial clearance in OVCA433 and OVCA432 cell lines, and reduction in these transcription factors increases the epithelial phenotype of ovarian tumor cells lines.

*Vimentin regulates mesothelial clearance ability*. Vimentin, an intermediate filament protein and downstream effector of EMT transcription factors (26), is enriched in the clearance-competent ovarian cancer cell lines (Figure 1). Because vimentin expression has been implicated in cell motility (35), we wanted to determine whether vimentin could also regulate mesothelial clearance. Vimentin expression was reduced in OVCA433 cells using siRNA SMARTpools, causing a downregulation of vimentin protein expression and significantly decreased clearance. (Figure 3, R and S, respectively). Furthermore, knockdown of vimentin using shRNA hairpins significantly decreased mesothelial clearance (Supplemental Figure 6) in a second cell line, CP70 (Supplemental Figure 7). Overall, these results are consistent with the possibility that EMT-mediated regulation of vimentin expression contributes to the ability of tumor cells to clear and invade mesothelium.

*Differential clearance ability in primary ovarian cancer cells from the ascites fluid of patients with ovarian cancer correlates with the expression of E-cadherin and vimentin*. To determine whether similar correlations between clearance activity and epithelial or mesenchymal phenotypes could be observed in primary ovarian cancer cell samples, we examined mesothelial clearance activity of primary serous papillary ovarian tumor cells derived from ascites fluid of 21 patients with high-grade serous ovarian cancer (DF9, DF14, DF24, DF29, DF43, DF59, DF68, DF106, DF118, DF141, DF143, DF147, DF155, DF160, DF163, DF164, DF166, DF168, DF172, DF173, DF176). Minimally processed frozen vials of primary ovarian cancer cells were plated on tissue culture plastic for 48 hours. The attached cells were trypsinized and divided into 3 aliquots. One aliquot was plated on untreated tissue culture plates for 24 hours and then lysed for Western blot and reverse-phase protein array (RPPA) analysis to measure the expression of epithelial and mesenchymal markers. A second aliquot was plated on poly-HEMA–coated culture dishes and grown in suspension for 24 hours before being lysed for marker analysis. The third aliquot was plated at 100 cells per well in 96-well poly-HEMA–coated culture dishes to form multicellular spheroids, and, after 16 hours in suspension, the spheroids were analyzed for clearance activity (Figure 4A). Cells from several representative clearance-competent DF cell populations (DF143, DF164, and DF163) were stained for PAX8, a Müllerian marker expressed by serous papillary ovarian tumors (36, 37), after spreading on mesothelial monolayers (Figure 4B) or glass (Supplemental Figure 9); all of these lines expressed nuclear PAX8, confirming the ovarian carcinoma origin of clearance-competent cells. After 8 hours of coculture in the mesothelial clearance assay, 14 of the primary cell lines were found to be clearance competent (normalized clearance area >1), while 7 of the primary cell populations were clearance incompetent (normalized clearance area <1) (Figure 4C, Supplemental Figure 8, and Supplemental Video 2). Quantification of the levels of expression of E-cadherin and vimentin from Western blot analyses revealed a significant enrichment of E-cadherin in the clearance-incompetent DF lines, while vimentin was enriched in the clearance-competent DF tumor cells (Figure 4, D–F). These results were very consistent with the findings from the established ovarian cancer cell lines.

We also examined the expression of E-cadherin and vimentin by immunofluorescent staining of sections from the cell blocks of the ascitic fluid from which the DF cell populations were derived (Figure 4G). Consistent with the Western blot data, ovarian cancer cells from DF174 and DF176, 2 clearance-incompetent cell populations, were positive for E-cadherin, but not vimentin, while ovarian cancer cells from DF164, a clearance-competent line, strongly stained for vimentin and only weakly stained for E-cadherin. The stromal and hematopoietic cells in samples DF147 and DF164 expressed high levels of vimentin. These cells were likely cleared by the filtration step that was used for processing the ascitic fluid samples, since there were low levels of vimentin in the cultured DF147 cells.

*Protein expression profile of clearance-competent and clearance-incompetent primary ovarian cancer spheroids*. To better characterize the primary tumor samples, the expression levels of 151 proteins and phosphoproteins representing major signaling pathways and some EMT marker proteins were measured in the 21 primary ovarian cancer cell populations using RPPA. To identify the proteins that are differentially expressed between primary cell populations with different levels of clearance activity, a multiple linear regression model was constructed using the normalized clearance area data from the mesothelial clearance assay and the relative protein expression data from the RPPA analysis. In this analysis, only cell populations with a clearance-competent value >2.5 or a clearance-incompetent value <1.0 were used, and the results are depicted in a heat map with the antibody probes that have a significant linear relationship ($P < 0.05$) with normalized clearance area (Figure 5A). Consistent with the above findings, epithelial proteins, including E-cadherin, claudin 7, and HER3, were enriched in the primary cell populations that displayed the weakest clearance activity. Mesenchymal markers are not well represented in the list of antibodies available for RPPA analysis, so the expression of mesenchymal proteins could not be evaluated in this analysis. However, YAP, which induces EMT when overexpressed in mammary epithelial cells (38), was strongly correlated with clearance-competent cell populations. The eEF2 and eEEF2 kinases were also enriched in this population.

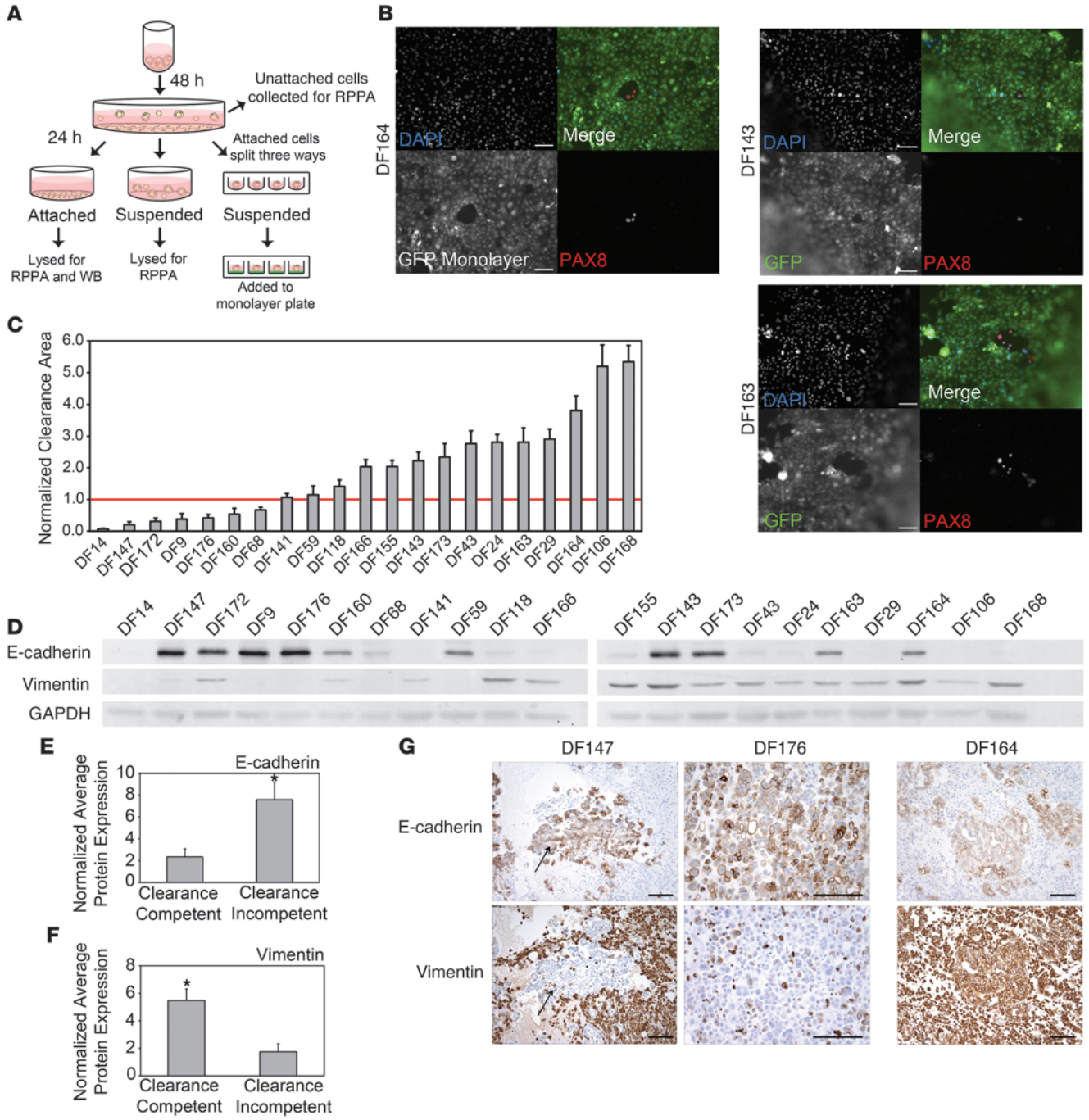


**Figure 4**

Spheroids from primary ovarian cancer cell lines display differential clearance ability that correlates with epithelial and mesenchymal marker expression. (**A**) Schematic outlining the treatment of the DF primary cell populations. (**B**) Representative images of immunofluorescence for PAX8 (red) and DAPI (blue) in DF164, DF143, and DF163 spheroids invading GFP-expressing (green) mesothelial monolayers for 8 hours. (**C**) Normalized clearance area was measured in 21 primary ovarian cancer cell populations. Samples with an average normalized clearance area >1 were characterized as clearance competent. Samples with an average normalized clearance area <1 were characterized as clearance incompetent. >20 spheroids were analyzed per condition. (**D**) Western blot analysis of E-cadherin and vimentin expression in 21 primary ovarian cancer cell lines. (**E** and **F**) Average (**E**) E-cadherin or (**F**) vimentin protein expression levels in clearance-competent and clearance-incompetent cell lines measured by densitometry. (**G**) Immunohistochemical analysis of sections from paraffin-embedded blocks of cells from the original ascitic fluid that the DF cell populations were derived from. Sections were stained with antibodies directed against E-cadherin or vimentin. Representative images from sections from clearance-incompetent (DF147 and DF176) and clearance-competent (DF164) primary cells. The E-cadherin and vimentin images from DF147 and DF164 were from the same area of the tumor; however, the tumor cells in the DF176 tumors were so discohesive that it was not feasible to find the same cells in both sections. All of the cell blocks were stained with PAX8 to confirm the Müllerian identity of the tumor cells (data not shown). Error bars denote SEM. *$P < 0.05$, Student's *t* test. Scale bar: 100 μm.

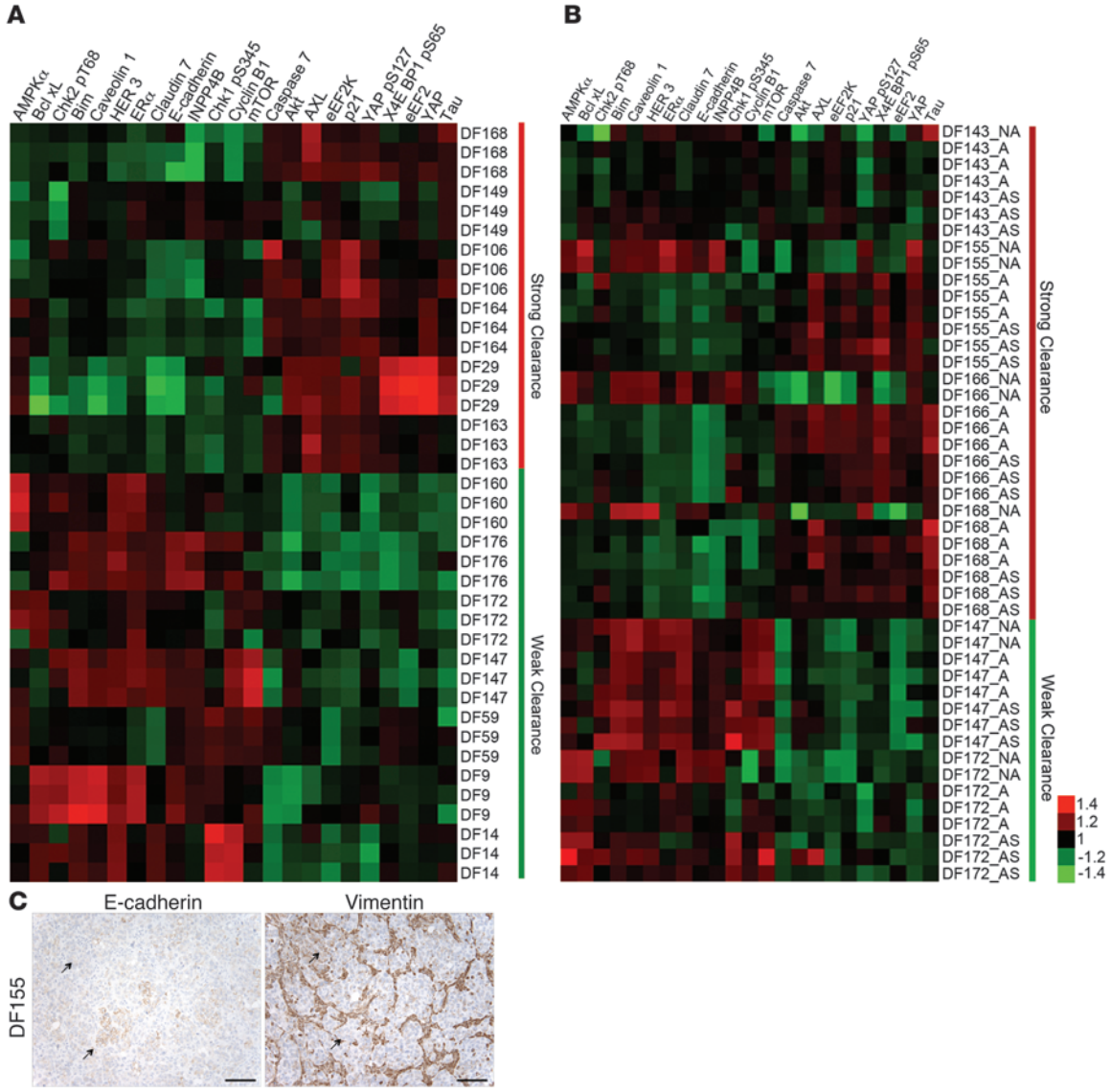


**Figure 5**

RPPA analysis reveals distinct populations of cells within some primary ovarian cancer cell lines. (**A**) RPPA analysis of the DF ovarian tumor cell populations. Antibodies that distinguish clearance-competent (normalized clearance area >2.5) and clearance-incompetent lines (normalized clearance area <1.0) are shown ($P < 0.05$, Student's $t$ test). (**B**) RPPA analysis of 4 clearance-competent and 2 clearance-incompetent ovarian cancer cell lines. Antibodies were chosen based on analysis in **A**. NA, population of cells that did not attach to the tissue culture dish 48 hours after thawing; A, population of cells that attached to the tissue culture dish 48 hours after thawing; AS, population of cells that attached to the tissue culture dish 48 hours after thawing followed by 24 hours of incubation in suspension in poly-HEMA–coated culture dishes. (**C**) Immunohistochemical analysis of sections from the primary tumor DF155, which were stained with antibodies directed against E-cadherin or vimentin. Scale bar: 100 μm.

The RPPA data described above were derived from primary ovarian cancer cells that were able to initially attach to a cell culture dish 48 hours after thawing from a stock vial. For several of the primary cell populations, a proportion of the cells were unable to attach to the culture dish after 48 hours. These nonadherent cells did not display activity in the mesothelial clearance assay (data not shown). Interestingly, the protein expression profiles of the nonattached cell populations derived from the clearance-competent cell populations were very similar to the protein expression profiles of the clearance-incompetent DF populations (being enriched for epithelial markers and other proteins in this signature) and clearly distinguished from cell populations of the same tumor that initially attached to tissue culture plates (Figure 5B). In contrast, for those tumors in which the attached cells were classified as clearance incompetent, the protein expression pattern of the unattached population and attached population of the same cell line were indistinguishable (Figure 5B).

Histologic sections from the DF155 primary tumor (one of the tumors in which the ascites samples displayed heterogeneous cell populations with differential abilities to attach to culture plates) stained for both E-cadherin and vimentin (Figure 5C). Both E-cadherin and vimentin were focally expressed in some, but not all,

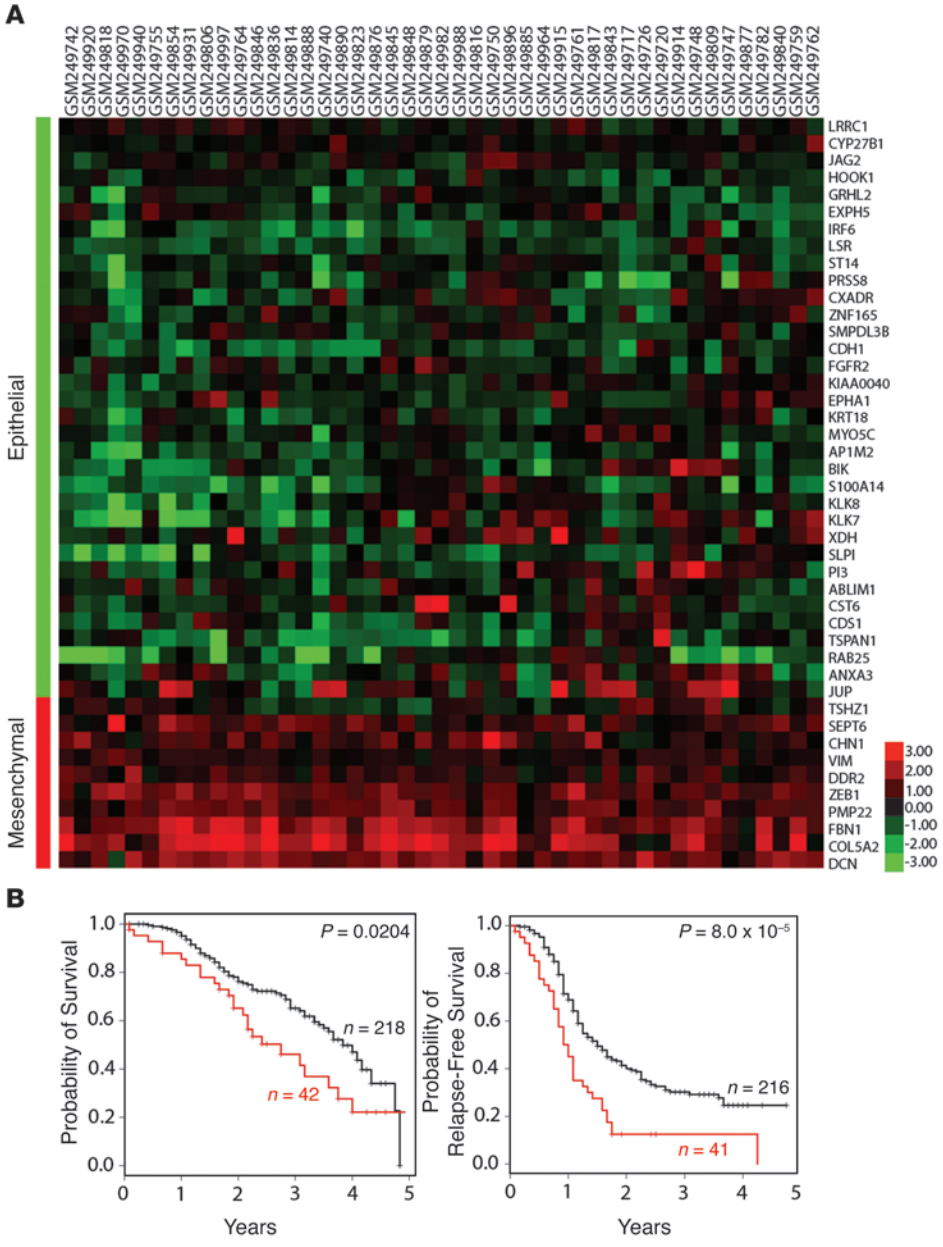


**Figure 6**
Mesenchymal gene signature in ovarian cancer data sets. (**A**) Samples in the Tothill ovarian data set (39) that significantly express the EMT signature in Figure 1 (Spearman's rho ≥ 0.295, $P < 0.05$). (**B**) Probability of 5-year survival and 5-year relapse-free survival in EMT signature overlapping (red) versus nonoverlapping (black) Tothill samples.

of the ovarian cancer cells. E-cadherin expression and vimentin expression were almost entirely mutually exclusive (Figure 5C, see arrows), supporting the existence of two distinct tumor populations. Taken together, these results suggest that primary ovarian cancer effusions contain a heterogeneous population of cells with differential ability to clear monolayers. The cells that exhibit mesenchymal markers display the strongest clearance activity.

*EMT gene signature in patients with epithelial ovarian cancer.* To address the significance of our findings to human ovarian cancer, we examined and compared the characteristics of our patient population to that of Tothill et al. (39). Tothill et al. used gene expression profiling to characterize 285 predominantly high-grade and advanced serous cancers of the ovary, fallopian tube, and peritoneum. A small number of endometrioid and low-grade serous tumors were also included in the analysis. They defined 6 subgroups (C1–C6) with distinct molecular and histopathologic characteristics (39). One subgroup (C5) expressed genes associated with mesenchymal development (including increased expression of homeobox genes, WNT/β-catenin pathway components, and N- and P-cadherin). When we compared the gene expression profiles of the ovarian tumors in the Tothill study to the clearance-associated EMT signature (Figure 1), we found that 16% (45 of 285) of the Tothill tumors expressed this EMT signature (Figure 6A). The median overall survival and relapse-free survival times were significantly shorter for patients bearing tumors with the EMT signature (Figure 6B). Interestingly, the majority of the 45 tumors that expressed our EMT signature did not fall into the Tothill "mesenchymal signature" C5 subgroup (3 of 45), but rather the tumors fell into the C1 "stromal signature" subgroup (34 of 45). Several of the genes that define our EMT signature were also found in the Tothill C1 "stromal signature" (*COL5A2*, *DCN*, *FBN1*, *ZEB1*, and *PMP22*). More importantly, C1 tumors were uniquely enriched for vimentin (average 2.14-fold) and had the poorest survival as a group compared with the other high-grade groups in the study. Interestingly, 8 of 18 of the DF cell populations that had available clinical information were derived from primary peritoneal tumors, and 7 of 8 of these expressed vimentin protein. In the Tothill study, 71% of the primary peritoneal carcinomas fell into the C1 subgroup compared with 25% (59 of 233) of cancers with an ovarian or tubal origin ($P \leq 0.0001$ by Fisher's exact test). Although we only had access to a limited amount of clinical data, which resulted in a small clinical sample size, this signature may be more common among primary peritoneal carcinomas and contribute to the poorer prognosis seen among primary peritoneal carcinomas compared with carcinomas from a primary ovarian or tubal tumor.

Taken together, our data suggest that vimentin expression identifies a population of tumor cells with an enhanced capacity to clear mesothelium. These tumors possess an EMT signature, which is associated with a poor clinical outcome.

## Discussion

In the current study, we conducted a comprehensive analysis of the gene and protein expression profiles of ovarian cancer spheroids with differential mesothelial clearance abilities. Using 20 established ovarian tumor cell lines, we identified a gene expression profile that correlated with mesothelial clearance activity. The expression of genes in an EMT core signature was enriched in the cell lines that showed strong mesothelial clearance activity compared with those with weak or undetectable activity, and manipulation of EMT transcription factors in these cell lines modulated the clearance activity as predicted. Importantly, this expression pattern was confirmed in primary tumor cell cultures using several EMT markers. Vimentin (a mesenchymal marker) was expressed at higher levels in primary tumor cells with high clearance activity, while E-cadherin, claudin 7, and HER3 (epithelial markers) expression was increased in primary cells with low clearance activity. These correlations were detected even in subpopulations within individual primary tumor cell samples. These studies provide clear insights into the molecular features that correlate with mesothelial invasive ability.

It has been proposed that cancer cells hijack EMT transcriptional programs to dissociate from the primary tumor and invade distant sites (26, 40–42). Ovarian cancer cells do not face these barriers in metastasizing to the peritoneum. Instead, they are displaced from primary tumors directly into the peritoneal cavity in which they can transit to other peritoneal tissues and then invade through the mesothelial lining to colonize new sites.

EMT has been implicated in ovarian carcinoma (43–45). It has been proposed that EMT is involved in the delamination of ovarian cancer cells from primary tumor sites, a process that would facilitate tumor dissemination. Cytokines present in ascitic effusions (e.g., VEGF, TNF-α, IL-6, IL-8, bFGF, lysophosphatidic acid) could also trigger or stabilize EMT through paracrine-autocrine loops). Several groups have shown that EMT markers, including α2β1 integrin, N-cadherin, and vimentin, can be upregulated in primary ovarian tumor spheroids when cultured in suspension in vitro (20, 45, 46). Our studies indicate that EMT would also enhance tumor cell invasion into the mesothelial layer of the peritoneal cavity. This would be consistent with the evidence that lower E-cadherin mRNA expression in ovarian carcinoma effusions correlates with poor survival (44). In addition, high expression of E-cadherin has been shown to be associated with better survival in a large recent study of high-grade serous ovarian carcinomas, with opposite findings for N-cadherin and P-cadherin (47)

Once attached to and spread on the peritoneum, ovarian cancer spheroids may undergo mesenchymal-to-epithelial transition, which is predicted to promote enhanced proliferation at the attachment site (43, 45, 48). Consistent with this prediction, E-cadherin expression was shown to be significantly elevated in metastatic ovarian lesions compared with that in their respective primary tumors (49).

Our studies indicate that EMT transcription factors promote mesothelial invasion by ovarian cancer cells. Overexpression of SNAI1, ZEB1, or TWIST1 in clearance-incompetent cell lines significantly ($P < 0.05$) increased mesothelial clearance ability. Conversely, inhibition of TWIST1 and ZEB1 in clearance-competent ovarian cancer cell lines significantly ($P < 0.05$) decreased mesothelial clearance. Previous reports have used in vitro migration assays to examine the role of EMT transcription factors in modulating other phenotypic aspects of the invasive behavior of ovarian tumor cell lines (reviewed in ref. 45). For example, downregulation of SNAI1 or TWIST1 expression in ES2 or HEY cells, respectively, suppressed invasion through Matrigel (50, 51). Similar differences in invasive behavior caused by EMT transcription factor modulation have been described in many other tumor cell lineages (reviewed in refs. 52, 53). A recent study reported a correlation among expression of CD157, an ectoenzyme regulating leukocyte diapedesis; expression of mesenchymal markers; and enhanced mesothelial invasion in ovarian cancer cells (54).

Recently, Kwon et al. correlated the ability of ovarian cancer spheroids to remodel extracellular matrices with the expression of epithelial and mesenchymal markers (55), dividing the cell lines into two groups: one that remodeled the ECM by degradation and one that remodeled the ECM by Rho-kinase–mediated (ROCK-mediated) reorganization. These investigators suggested that ovarian cancer cells could use two distinct strategies to remodel ECM during ovarian cancer metastasis. Interestingly, the cell lines that used ROCK-mediated reorganization of the ECM expressed mesenchymal markers, including N-cadherin and vimentin, while cell lines that remodeled the ECM via degradation expressed epithelial markers, including E-cadherin and pan-keratin.

Based on these data and our previous report showing that myosin II, which is a substrate of ROCK, is required for mesothelial clearance (24), it is plausible to hypothesize that ROCK-dependent regulation of myosin II is required for mesenchymal ovarian cancer spheroids to invade mesothelial monolayers.

While we have shown that tumor cells expressing genes associated with a mesenchymal program display more effective mesothelial clearance in vitro, the contribution of these cells to ovarian cancer progression remains unclear. Studies have found that higher SNAI1 or TWIST1 expression in primary ovarian carcinomas, ovarian cancer effusions, and metastases is associated with shorter overall and progression-free survival (reviewed in ref. 43). In addition, the expression of SNAI1 and TWIST1 is significantly higher in later stage ovarian tumors (III and IV) compared with that in early-stage ovarian tumors (reviewed in ref. 43). Consistently, increased expression of E-cadherin is associated with better survival, while loss of E-cadherin expression is associated with poor survival in several studies (reviewed in refs. 43, 45).

Vimentin and E-cadherin expression may also reflect the carcinoma site of origin. While collectively referred to as "ovarian cancers," serous carcinomas may originate from the ovary itself, the fallopian tube, or the peritoneum. Pathologists classify serous tumors by the most likely primary site. Once considered a rare tumor, the fallopian tube is now considered the site of origin for most serous tumors (56–59). Primary peritoneal carcinomas, however, continue to be uncommon, accounting for about 15% of serous carcinomas. These tumors are diagnosed when the fallopian tubes and ovaries are surgically absent or when all sites seen are consistent with metastatic foci and no dominant mass or precursor lesion is evident in the ovaries or fallopian tubes. Among the 21 patients from whom the DF cell lines were derived, 18 had clinical information regarding the primary site (2 patients never had surgical staging, and 1 patient did not consent to her clinical information being used).

8 of 18 (44%) of these patients were diagnosed with a primary peritoneal carcinoma, and all but one of the DF cell lines derived from a primary peritoneal carcinoma expressed vimentin.

Interestingly, in the report by Tothill et al. (39), primary peritoneal carcinomas were much more likely to correspond to the C1 molecular subtype than primary tubal or ovarian serous carcinomas. 71% (24 of 34) of primary peritoneal cancers examined in the Tothill et al. study were characterized as C1 subtype cancers, while only 25% (59 of 233) of primary ovarian or tubal cancers were characterized as C1 subtype cancers ($P < 0.0001$ by Fisher's exact test). Relevant to our study, the C1 molecular subtype was unique among the 6 subsets described by Tothill in the increased expression of vimentin (by an average of 2.14-fold). The C1 molecular subtype was also associated with the poorest progression-free and overall survival among the high-grade molecular subtypes they identified. This may be consistent with a study showing that patients with primary peritoneal carcinomas fare worse than patients with serous carcinomas from other primary sites (60).

The decreased survival in our EMT signature tumor subgroup may be due, at least in part, to the increased ability of these cells to invade the mesothelial lining of peritoneal cavity organs. However, given that ovarian tumors show intratumoral heterogeneity with respect to epithelial and mesenchymal markers (as detected in tumor DF155 in our study), analyses involving RNA or protein expression of the total population of cells may mask the existence of mesenchymal cells that could contribute to mesothelial clearance. It remains to be established whether inhibitors that block intercalation will be useful clinically in preventing new metastases. The potential associated complications following surgical debulking of peritoneal masses will also need to be evaluated.

Our study provides insight into the molecular mechanisms that mediate mesothelial clearance by ovarian cancer multicellular spheroids. We have shown that ovarian cancer spheroids displaying mesenchymal characteristics are more efficient at clearing a mesothelial monolayer. Furthermore, we found heterogeneity with respect to the expression of mesenchymal markers and competence for mesothelial clearance in primary tumor populations. These studies raise the possibility that inhibition of the mesenchymal program could reduce seeding of new ovarian cancer metastatic lesions following surgical debulking.

## Methods

### *Cell culture*

*Established cell lines*. All of the established ovarian cancer cell lines, as well as the ZT mesothelial cells, were cultured in a 1:1 ratio of medium MCDB 105 (Cell Applications Inc.) and Medium 199 (GIBCO) supplemented with 10% FBS (GIBCO) and 5% penicillin-streptomycin (GIBCO). The established ovarian cancer cell lines were provided by Dennis J. Slamon. ZT mesothelial cells were obtained from a benign pleural effusion. These cells were immortalized by ectopic expression of SV40 T antigen and overexpression of human telomerase (fused to GFP), as previously described (61).

*Primary tumor cells*. Under institutional review board approval (Dana-Farber/Harvard Cancer Center Review Board, Boston, Massachusetts, USA; IRB no. 02-051) and with informed consent, primary ovarian carcinoma cells (DF lines) were isolated directly from peritoneal paracentesis of patients with advanced-stage ovarian cancer at the time of initial cytoreductive surgery, as previously described (62). Red blood cells were lysed, as previously described (62), and only samples that were >80% pure tumor cells were used. In cases in which there was more heterogeneity, the samples were enriched for tumor cells by filtration using a 40-μm nylon cell strainer (BD Falcon) to isolate tumor cell spheres. Tumor cells were frozen after isolation, and aliquots were thawed and cultured in WIT- medium optimized for ovarian tumor cells as needed for the experiments described.

### *Mesothelial clearance assay*

*Preparation of spheroids and mesothelial monolayer*. The mesothelial clearance assay was performed as previously described (24) with minor alterations. Briefly, to generate multicellular spheroids, ovarian cancer cells were dissociated by trypsinization, resuspended in cell culture medium, and counted. 100 cells per well were plated in poly-HEMA–coated 96-well round bottom plates (Corning), and the plates were incubated at 37°C for 16 hours to promote spheroid formation. Concurrently, 5,000 ZT mesothelial cells per well were plated on fibronectin-coated (5 μg/ml, Sigma-Aldrich) 384-well glass-bottom culture dishes (Corning). The mesothelial cells were incubated at 37°C for 16 hours to form confluent monolayers. After the 16-hour incubations, the ovarian cancer multicellular spheroids were transferred to the wells containing the mesothelial monolayers.

*Live cell imaging*. Imaging was performed using a Nikon Ti-E Inverted Motorized Widefield Fluorescence Microscope with the integrated Perfect Focus System and low (×20, 0.75 NA) magnification/NA DIC optics, Nikon halogen transilluminator with 0.52 NA LWD condenser, Nikon fast (<100-ms switching time) excitation and emission filter wheels, Sutter fast transmitted and epifluorescence light path Smart shutters, Nikon linear-encoded motorized stage, Hamamatsu ORCA-AG cooled CCD camera, custom-built microscope incubation chamber with temperature and $CO_2$ control, Nikon NIS Elements AR software v3, and TMC vibration-isolation table. Over 20 spheroids were imaged per condition. Phase-contrast and GFP images were captured every 10 minutes for 8 hours.

*Quantification of mesothelial clearance area*. The nonfluorescent area, created by the invading spheroid, in the GFP mesothelial monolayer images was measured at 8 hours and divided by the initial area of the cancer spheroid at time 0. All measurements were taken using Nikon NIS Elements software.

*Quantification of percent hole formation*. For each condition, after 8 hours of coincubation, the number of positions with a mesothelial clearance area >1 were counted, divided by the total number of positions, and multiplied by 100.

### *Microarray analysis*

Microarray hybridizations were performed in the ovarian cell lines at baseline using the Agilent Human 44K array chip. Briefly, cells were grown to log phase and then RNA was extracted using the RNeasy Kit (Qiagen). The purified RNA was eluted in 30 to 60 μl diethylpyrocarbonate water, and the quantity of RNA was measured by spectral analysis using the Nanodrop Spectrophotometer (NanoDrop Products). RNA quality was determined by separation of the RNA via capillary electrophoresis using the Agilent 2000 Bioanalyzer (Agilent Technologies). Characterization of individual ovarian cancer cell line transcripts was performed by comparison to a mixed reference cRNA pool consisting of equal amounts of RNA from 40 ovarian cancer cell lines and was conducted on a single microarray slide in which the cell line mixture RNA was labeled with cyanine-3 and RNA from the individual cell line was labeled with cyanine-5. Microarray slides were read using an Agilent Scanner, and the Agilent Feature Extraction software version 7.5 was used to calculate gene expression values. Data were prefiltered using a $P$ value threshold of $P < 0.01$ in at least one cell line, and differentially expressed genes were identified using the limma package of bioConductor R and a $P$ value threshold of 0.05. Microarray data are available at the GEO (GEO accession no. GSE26805).

Enrichment was assessed in two ways: (a) differentially expressed genes were assessed for enrichment of GeneGO categories using GeneGO software (http://www.genego.com) or (b) the differentially expressed genes

were merged to an EMT signature consisting of the Taube EMT core signature (25) and 6 additional transcription factors (*SNAI1*, *SNAI2*, *ZEB2*, *TWIST1*, *TWIST2*, *OVOL1*). The background population set was 15,900 unique genes after prefiltering the ovarian cell line expression data. Enrichment *P* values were calculated with hypergeometric distribution implemented in the phyper function in R. Fold enrichment was defined as the observed frequency divided by the expected frequency. Hierarchical cluster diagrams were built using a Pearson uncentered distance measure with average linkage rules in Cluster (v.3.0) and then visualized in Java Tree View (v1.1.0).

### *Five-year survival analysis*

The EMT signature was merged to the Tothill data downloaded from GEO (GEO accession no. GSE9891) (39) using Affymetrix gene identifiers. In order to deal with multiple probes per gene, the probe with the highest variance was selected. Only patients with a follow-up time of less than 5 years were included in the survival analysis. Patients were divided into 2 groups based on correlation or lack of correlation with the EMT signature; samples with the EMT signature were defined as Spearman $\rho \geq 0.295$ ($P < 0.05$). Kaplan-Meier curves were generated using the survival package in R. Log-rank *P* values were computed with the survdiff function.

### *Western blot analysis*

Cells were lysed in RIPA buffer (50 mM HEPES pH 7.4, 1% Triton X-100, 1% sodium deoxycholate, 0.1% SDS, 0.1 M NaCl, 1 mM sodium orthovanadate, 0.1 M sodium pyrophosphate, 100 mM NaF, and 1 mM PMSF). Lysates were clarified by centrifugation at 13,000 *g* for 10 minutes at 4°C, protein concentration was quantified using the BCA assay (Pierce), and absorbance was read on a BioTEK Micro-Volume Spectrophotometer System (Epoch). 15 μg lysates were boiled in 1× sample buffer (0.04 M Tris-HCl pH 6.8, 1% SDS, 1% β-mercaptoethanol, and 10% glycerol) for 10 minutes and resolved by SDS-PAGE. Proteins were transferred to Immobilon membranes (Whatman) and blocked with 5% BSA in PBS (140 mM NaCl, 0.27 mM KCl, 0.43 mM $Na_2HPO_4$, 0.14 mM $KH_2PO_4$ pH 7.3) for 30 minutes at room temperature. Membranes were incubated overnight at 4°C with one or more of the following antibodies: anti–E-cadherin monoclonal antibody (1:1,000, BD), anti-vimentin polyclonal antibody (1:1,000, Cell Signaling), anti-GAPDH polyclonal antibody (1:20,000, Abcam), or anti-tubulin polyclonal antibody (1:20,000, Abcam). Membranes were then probed with secondary antibodies linked to HRP (1:5000, Santa Cruz) or secondary antibodies linked to fluorophores (1:5,000, LI-COR). Western blot membranes incubated with HRP were developed using an enhanced chemiluminescent substrate (VWR) and visualized using a Kodak film developer and an Epson 3000 scanner. Fluorophore-treated Western blot membranes were visualized using the Odyssey Imaging System (LI-COR Biosciences). Protein expression levels were quantified from the Western blot membranes visualized using the Odyssey imaging system by measuring the mean pixel density of the band in question using ImageJ software and dividing by the mean pixel density of the corresponding loading control band.

### *cDNA plasmids, siRNAs, shRNAs*

To ectopically express TWIST1 or SNAI1, the retroviral vector (pWZL Blast ER) encoding the genes for TWIST1 or SNAI1 was transfected into MCAS ovarian cancer cells (Addgene plasmids 18799 and 18798, respectively). Cells were selected in 50 μg/ml blasticidin and induced with 20 nM 4-OHT for 7 days. To ectopically express ZEB1, aTET-ON system was used: MCAS cells were first transfected with pBABE-rtTA and selected with 50 μg/ml hygromycin B. MCAS cells stably expressing rtTA were then transfected with the lentiviral vector pFUW-LPT2-ZEB1 and selected in 100 μg/ml puromycin. ZEB1 expression was induced with 1 μg/μl doxycycline for 7 days. siRNA SMARTpools against TWIST1, TWIST2, ZEB1, ZEB2, vimentin, and E-cadherin were used to attenuate the expression of the corresponding genes (Dharmacon). Lentiviruses lacking an shRNA sequence (pLKO), as a control, or plasmids containing TWIST1 hairpins (OpenBiosystems; G11 seq: 5′-CCGGCGCCTTCTCGGTCTGGAGGATCTCGAGATCCTCCAGACCGAGAAGGCGTTTTT-3′, G12 seq: 5′-CCGGTCCGCAGTCTTACGAGGAGCTCTCGAGAGCTCCTCGTAAGACTGCGGATTTTT-3′) were used to attenuate the expression of TWIST1 in OVCA433 cells. pLKO, as a control, or plasmids containing vimentin hairpins (OpenBiosystems; A11 seq: 5′-CCGGGCTAACTACCAAGACACTATTCTCGAGAATAGTGTCTTGGTAGTTAGCTTTTT-3′, B1 seq: 5′-CCGGGCAGGATGAGATTCAGAATATCTCGAGATATTCTGAATCTCATCCTGCTTTTT-3′, B2 seq: 5′-CCGGCGCCATCAACACCGAGTTCAACTCGAGTTGAACTCGGTGTTGATGGCGTTTTT-3′, B3 seq: 5′-CCGGGACAGGTTATCAACGAAACTTCTCGAGAAGTTTCGTTGATAACCTGTCTTTTT-3′) were used to attenuate the expression of vimentin in OVCA433 cells. pLKO, as a control, or plasmids containing ZEB1 hairpins (Arizona State University; 1 seq: CCGGGCAACAATACAAGAGGTTAAACTCGAGTTTAACCTCTTGTATTGTTGCTTTTT, 2 seq: CCGGGCTGCCAATAAGCAAACGATTCTCGAGAATCGTTTGCTTATTGGCAGCTTTTT, 3 seq: CCGGCCTCTCTGAAAGAACACATTACTCGAGTAATGTGTTCTTTCAGAGAGGTTTTT, 4 seq: CCGGGCTGTTGTTCTGCCAACAGTTCTCGAGAACTGTTGGCAGAACAACAGCTTTTT) were used to attenuate the expression of ZEB1 in OVCA433 cells. Lentivirus-infected cells were selected in medium containing 1 μg/ml puromycin (Dulbecco).

### *Quantitative real-time PCR*

RNA was isolated from ovarian cancer cells using the TRIzol reagent (Invitrogen) according to the manufacturer's instructions. The RNA was reverse transcribed into cDNA using the qScript cDNA Synthesis Kit (Quanta) according to the manufacturer's instructions. cDNA levels were quantitated by the SYBR green method on the T900HT (Life Technologies) in a 384-well format. Triplicate samples were quantified along with minus reverse transcriptase and minus template controls. Amplification was continued for 40 cycles as follows: 94°C for 10 seconds, 55°C for 15 seconds, 65°C for 30 seconds. Relative expression was determined by normalizing to the PRLPO endogenous control.

### *RPPA*

A vial of primary ovarian cancer cells from each of the DF lines was thawed and plated on 10-cm cell culture dishes. After 48 hours, the attached cells were trypsinized and split into 3 wells of a 6-well cell culture dish. Cells were allowed to reattach overnight to form confluent monolayers. RPPA analysis was performed as previously described (63). Briefly, cells were collected by washing with ice-cold PBS, scrapping, and centrifugation at 900 *g* at 4°C for 10 minutes. Pellets were resuspended in RPPA lysis buffer (1% Triton X-100, 50 mM HEPES pH 7.4, 150 mM NaCl, 1.5 mM $MgCl_2$, 1 mM EGTA, 100 mM NaF, 10 mM NaPPi, 10% glycerol, 1 mM $Na_3VO_4$, and protease inhibitor [Roche]) and incubated on ice with occasional shaking for 20 minutes. The lysates were centrifuged at 13,000 *g*, 4°C, for 10 minutes. Lysed were denatured by adding 1% SDS and boiling for 5 minutes. Each sample was diluted in five 2-fold serial dilutions and printed onto nitrocellulose-coated glass slides (Grace Biolabs) with an automated robotic Aushon arrayer (Aushon Biosystems). Each slide was probed with a validated primary and secondary antibody, as described previously (63); 151 antibodies were used in total. Signal intensity was measured by scanning the slides with ImageQuant (Molecular Dynamics) and quantified using the MicroVigene automated RPPA module (VigeneTech Inc.).

Relative protein levels were then determined for each sample. Signal intensity data were collected and analyzed using software developed specifically for RPPA analyses (http://www.VigeneTech.com). Log-transformed intensity data were subjected to Student's *t* tests in bioConductor R. Significant antibody probes were defined as $P < 0.05$. Log-transformed and centered heat maps were generated using Cluster 3.0 and Java TreeView 1.1.1.

### *Immunohistochemistry*

After institutional review board approval (Dana-Farber/Harvard Cancer Center Review Board), sections of formalin-fixed, paraffin-embedded cell blocks were obtained from the Cytology Division in the Department of Pathology at the Brigham and Women's Hospital to evaluate the expression of vimentin and E-cadherin. The prepared blocks corresponded to the ascites from the DF lines used in this study. Immunohistochemistry was performed using the Envision Plus/HRP system (Dako) and a polyclonal/monoclonal antibody to vimentin (Dako, clone 3B4, 1:400) and E-cadherin (Dako, clone NCH-38, 1:75) as previously described (36, 62). In brief, paraffin-embedded sections were incubated in hydrogen peroxidase and absolute alcohol for 30 minutes to block endogenous peroxidase activity. Antigen retrieval was performed using pressure cooker pretreatment in a citrate buffer (pH 6.0). Tissue sections were subsequently incubated with the primary antibody for 40 minutes at 25°C. After tris-buffered saline rinses, the tissue was incubated using the Envision Plus secondary antibody for 30 minutes followed by diaminobenzidine for 5 minutes. Slides were counterstained with Mayer hematoxylin.

### *Immunofluorescence*

Cells were fixed with 4% formaldehyde, permeabilized with 0.1% Triton X-100, and blocked with blocking buffer (10% BSA and 1% goat serum in PBS) for 1 hour. Cells were then incubated with anti-PAX8 antibody (1:200, Proteintech) for 1 hour followed by anti-mouse Alexa Fluor 568 secondary antibody (1:300, Invitrogen) for 1 hour. Cells were counterstained with DAPI for 15 minutes to visualize nuclei. Imaging was performed using a Nikon Ti-E Inverted Motorized Widefield Fluorescence Microscope as described above.

### *Statistics*

Two-tailed Student's *t* tests were used for all statistical analyses unless otherwise specified. *P* values of less than 0.05 were considered significant.

## Acknowledgments

We would like to thank Yiling Lu and Doris Siwak (MD Anderson Cancer Center) for performing the RPPA studies; Jennifer Waters and the Nikon Imaging Center at Harvard Medical School for support on the microscopy studies; and Kong-Jie Kah and Robert Weinberg for donation of the ZEB1 overexpression construct. We also thank Ghassan Mouneimne for review of the manuscript and helpful discussions and Grace Gao for lab management. These studies were supported by the Dr. Miriam and Sheldon G. Adelson Medical Research Foundation (to J.S. Brugge and R. Drapkin), the Ovarian Cancer Research Fund (to R. Drapkin), the Honorable Tina Brozman Foundation (to R. Drapkin), the Robert and Debra First Fund (to R. Drapkin), the Gamel Family Ovarian Cancer Research Fund (to R. Drapkin), the Susan F. Smith Center for Women's Cancers at the Dana-Farber Cancer Institute (to R. Drapkin), and the Men's Collaborative to Cure Women's Cancer (to J.S. Brugge and R. Drapkin). RPPA was performed at the MD Anderson RPPA Core Facility (supported by NIH grant CA016672).

Received for publication March 15, 2013, and accepted in revised form February 27, 2014.

Address correspondence to: Joan S. Brugge, Department of Cell Biology, Harvard Medical School, 240 Longwood Avenue, Boston, Massachusetts 02115, USA. Phone: 617.432.3974; Fax: 617.432.3969; E-mail: Joan_Brugge@hms.harvard.edu. Or to: Ronny Drapkin, Dana-Farber Cancer Institute, 450 Brookline Avenue, Boston, Massachusetts 02215, USA. Phone: 617.632.4380; Fax: 617.582.8761; E-mail: ronny_drapkin@dfci.harvard.edu.

1. Siegel R, Naishadham D, Jemal A. Cancer statistics, 2012. *CA Cancer J Clin*. 2012;62(1):10–29.
2. Cannistra SA. Cancer of the ovary. *N Engl J Med*. 2004; 351(24):2519–2529.
3. Shield K, Ackland ML, Ahmed N, Rice GE. Multicellular spheroids in ovarian cancer metastases: biology and pathology. *Gynecol Oncol*. 2009; 113(1):143–148.
4. Naora H, Montell DJ. Ovarian cancer metastasis: integrating insights from disparate model organisms. *Nat Rev Cancer*. 2005;5(5):355–366.
5. Sehouli J, et al. Intra-abdominal tumor dissemination pattern and surgical outcome in 214 patients with primary ovarian cancer. *J Surg Oncol*. 2009; 99(7):424–427.
6. Birbeck MS, Wheatley DN. An electron microscopic study of the invasion of ascites tumor cells into the abdominal wall. *Cancer Res*. 1965;25:490–497.
7. Witz CA, Monotoya-Rodriguez IA, Schenken RS. Whole explants of peritoneum and endometrium: a novel model of the early endometriosis lesion. *Fertil Steril*. 1999;71(1):56–60.
8. Zhang XY, Pettengell R, Nasiri N, Kalia V, Dalgleish AG, Barton DP. Characteristics and growth patterns of human peritoneal mesothelial cells: comparison between advanced epithelial ovarian cancer and non-ovarian cancer sources. *J Soc Gynecol Investig*. 1999;6(6):333–340.
9. Burleson KM, et al. Ovarian carcinoma ascites spheroids adhere to extracellular matrix components and mesothelial cell monolayers. *Gynecol Oncol*. 2004;93(1):170–181.
10. Kenny HA, Nieman KM, Mitra AK, Lengyel E. The first line of intra-abdominal metastatic attack: breaching the mesothelial cell layer. *Cancer Discovery*. 2011;1(2):100–102.
11. Kenny HA, et al. Organotypic models of metastasis: A three-dimensional culture mimicking the human peritoneum and omentum for the study of the early steps of ovarian cancer metastasis. *Cancer Treat Res*. 2009;149:335–351.
12. Niedbala MJ, Crickard K, Bernacki RJ. Interactions of human ovarian tumor cells with human mesothelial cells grown on extracellular matrix. An in vitro model system for studying tumor cell adhesion and invasion. *Exp Cell Res*. 1985;160(2):499–513.
13. Burleson KM, Boente MP, Pambuccian SE, Skubitz AP. Disaggregation and invasion of ovarian carcinoma ascites spheroids. *J Transl Med*. 2006;4:6.
14. Burleson KM, Hansen LK, Skubitz AP. Ovarian carcinoma spheroids disaggregate on type I collagen and invade live human mesothelial cell monolayers. *Clin Exp Metastasis*. 2004;21(8):685–697.
15. Ahmed N, Riley C, Rice G, Quinn M. Role of integrin receptors for fibronectin, collagen and laminin in the regulation of ovarian carcinoma functions in response to a matrix microenvironment. *Clin Exp Metastasis*. 2005;22(5):391–402.
16. Lessan K, Aguiar DJ, Oegema T, Siebenson L, Skubitz AP. CD44 and beta1 integrin mediate ovarian carcinoma cell adhesion to peritoneal mesothelial cells. *Am J Pathol*. 1999;154(5):1525–1537.
17. Strobel T, Cannistra SA. Beta1-integrins partly mediate binding of ovarian cancer cells to peritoneal mesothelium in vitro. *Gynecol Oncol*. 1999; 73(3):362–367.
18. Heyman L, Kellouche S, Fernandes J, Dutoit S, Poulain L, Carreiras F. Vitronectin and its receptors partly mediate adhesion of ovarian cancer cells to peritoneal mesothelium in vitro. *Tumour Biol*. 2008;29(4):231–244.
19. Cannistra SA, Kansas GS, Niloff J, DeFranzo B, Kim Y, Ottensmeier C. Binding of ovarian cancer cells to peritoneal mesothelium in vitro is partly mediated by CD44H. *Cancer Res*. 1993;53(16):3830–3838.
20. Shield K, Riley C, Quinn MA, Rice GE, Ackland ML, Ahmed N. α2β1 Integrin affects metastatic potential of ovarian carcinoma spheroids by supporting disaggregation and proteolysis. *J Carcinog*. 2007;6:11.
21. Kenny HA, Krausz T, Yamada SD, Lengyel E. Use of a novel 3D culture model to elucidate the role of mesothelial cells, fibroblasts and extra-cellular matrices on adhesion and invasion of ovarian cancer cells to the omentum. *Int J Cancer*. 2007; 121(7):1463–1472.
22. Slack-Davis JK, Atkins KA, Harrer C, Hershey ED, Conaway M. Vascular cell adhesion molecule-1 is a regulator of ovarian cancer peritoneal metastasis. *Cancer Res*. 2009;69(4):1469–1476.
23. Casey RC, et al. Establishment of an in vitro assay to measure the invasion of ovarian carcinoma cells through mesothelial cell monolayers. *Clin Exp Metastasis*. 2003;20(4):343–356.
24. Iwanicki M, et al. Ovarian cancer spheroids use myosin-generated force to clear the mesothelium. *Cancer Discovery*. 2011;1(2):144–157.
25. Taube JH, et al. Core epithelial-to-mesenchymal transition interactome gene-expression signature is

associated with claudin-low and metaplastic breast cancer subtypes. *Proc Natl Acad Sci U S A*. 2010; 107(35):15449–15454.
26. Kalluri R, Weinberg RA. The basics of epithelial-mesenchymal transition. *J Clin Invest*. 2009; 119(6):1420–1428.
27. Nakayama K, et al. Sequence mutations and amplification of PIK3CA and AKT2 genes in purified ovarian serous neoplasms. *Cancer Biol Ther*. 2006; 5(7):779–785.
28. Cano A, et al. The transcription factor snail controls epithelial-mesenchymal transitions by repressing E-cadherin expression. *Nat Cell Biol*. 2000; 2(2):76–83.
29. Vega S, Morales AV, Ocana OH, Valdes F, Fabregat I, Nieto MA. Snail blocks the cell cycle and confers resistance to cell death. *Genes Dev*. 2004; 18(10):1131–1143.
30. Mejlvang J, et al. Direct repression of cyclin D1 by SIP1 attenuates cell cycle progression in cells undergoing an epithelial mesenchymal transition. *Mol Biol Cell*. 2007;18(11):4615–4624.
31. Evdokimova V, Tognon C, Ng T, Sorensen PH. Reduced proliferation and enhanced migration: two sides of the same coin? Molecular mechanisms of metastatic progression by YB-1. *Cell Cycle*. 2009; 8(18):2901–2906.
32. Tsai JH, Donaher JL, Murphy DA, Chau S, Yang J. Spatiotemporal regulation of epithelial-mesenchymal transition is essential for squamous cell carcinoma metastasis. *Cancer Cell*. 2012;22(6):725–736.
33. Casas E, Kim J, Bendesky A, Ohno-Machado L, Wolfe CJ, Yang J. Snail2 is an essential mediator of Twist1-induced epithelial mesenchymal transition and metastasis. *Cancer Res*. 2011;71(1):245–254.
34. Cieply B, et al. Suppression of the epithelial-mesenchymal transition by Grainyhead-like-2. *Cancer Res*. 2012;72(9):2440–2453.
35. Mendez MG, Kojima S, Goldman RD. Vimentin induces changes in cell shape, motility, and adhesion during the epithelial to mesenchymal transition. *FASEB J*. 2010;24(6):1838–1851.
36. Laury AR, et al. A comprehensive analysis of PAX8 expression in human epithelial tumors. *Am J Surg Pathol*. 2011;35(6):816–826.
37. Karst AM, Levanon K, Drapkin R. Modeling high-grade serous ovarian carcinogenesis from the fallopian tube. *Proc Natl Acad Sci U S A*. 2011; 108(18):7547–7552.
38. Overholtzer M, et al. Transforming properties of YAP, a candidate oncogene on the chromosome 11q22 amplicon. *Proc Natl Acad Sci U S A*. 2006; 103(33):12405–12410.
39. Tothill RW, et al. Novel molecular subtypes of serous and endometrioid ovarian cancer linked to clinical outcome. *Clin Cancer Res*. 2008; 14(16):5198–5208.
40. Singh RP, Raina K, Sharma G, Agarwal R. Silibinin inhibits established prostate tumor growth, progression, invasion, and metastasis and suppresses tumor angiogenesis and epithelial-mesenchymal transition in transgenic adenocarcinoma of the mouse prostate model mice. *Clin Cancer Res*. 2008; 14(23):7773–7780.
41. Tsuji T, et al. Epithelial-mesenchymal transition induced by growth suppressor p12CDK2-AP1 promotes tumor cell local invasion but suppresses distant colony growth. *Cancer Res*. 2008;68(24):10377–10386.
42. Ota I, Li XY, Hu Y, Weiss SJ. Induction of a MT1-MMP and MT2-MMP-dependent basement membrane transmigration program in cancer cells by Snail1. *Proc Natl Acad Sci U S A*. 2009; 106(48):20318–20323.
43. Davidson B, Trope CG, Reich R. Epithelial-mesenchymal transition in ovarian carcinoma. *Front Oncol*. 2012;2:33.
44. Elloul S, et al. Snail, Slug, and Smad-interacting protein 1 as novel parameters of disease aggressiveness in metastatic ovarian and breast carcinoma. *Cancer*. 2005;103(8):1631–1643.
45. Ahmed N, Thompson EW, Quinn MA. Epithelial-mesenchymal interconversions in normal ovarian surface epithelium and ovarian carcinomas: an exception to the norm. *J Cell Physiol*. 2007; 213(3):581–588.
46. Valles AM, Boyer B, Tarone G, Thiery JP. α2β1 Integrin is required for the collagen and FGF-1 induced cell dispersion in a rat bladder carcinoma cell line. *Cell Adhes Commun*. 1996;4(3):187–199.
47. Quattrocchi L, Green AR, Martin S, Durrant L, Deen S. The cadherin switch in ovarian high-grade serous carcinoma is associated with disease progression. *Virchows Arch*. 2011;459(1):21–29.
48. Christiansen JJ, Rajasekaran AK. Reassessing epithelial to mesenchymal transition as a prerequisite for carcinoma invasion and metastasis. *Cancer Res*. 2006;66(17):8319–8326.
49. Davidson B, et al. E-cadherin and α-, β-, and γ-catenin protein expression is up-regulated in ovarian carcinoma cells in serous effusions. *J Pathol*. 2000; 192(4):460–469.
50. Elloul S, Vaksman O, Stavnes HT, Trope CG, Davidson B, Reich R. Mesenchymal-to-epithelial transition determinants as characteristics of ovarian carcinoma effusions. *Clin Exp Metastasis*. 2010; 27(3):161–172.
51. Terauchi M, et al. Possible involvement of TWIST in enhanced peritoneal metastasis of epithelial ovarian carcinoma. *Clin Exp Metastasis*. 2007; 24(5):329–339.
52. Nieto MA. The ins and outs of the epithelial to mesenchymal transition in health and disease. *Annu Rev Cell Dev Biol*. 2011;27:347–376.
53. Lee JM, Dedhar S, Kalluri R, Thompson EW. The epithelial-mesenchymal transition: new insights in signaling, development, and disease. *J Cell Biol*. 2006; 172(7):973–981.
54. Morone S, et al. Overexpression of CD157 contributes to epithelial ovarian cancer progression by promoting mesenchymal differentiation. *PLoS One*. 2012;7(8):e43649.
55. Kwon Y, Cukierman E, Godwin AK. Differential expressions of adhesive molecules and proteases define mechanisms of ovarian tumor cell matrix penetration/invasion. *PLoS One*. 2011;6(4):e18872.
56. Nik NN, Vang R, Shih IeM, Kurman RJ. Origin and pathogenesis of pelvic (ovarian, tubal, and primary peritoneal) serous carcinoma. *Annu Rev Pathol*. 2014; 9:27–45.
57. Piek JM, Verheijen RH, van Diest PJ. Tubal and ovarian pathways to pelvic epithelial cancer: a pathological perspective. *Histopathology*. 2009; 54(4):494–495.
58. Mehrad M, Ning G, Chen EY, Mehra KK, Crum CP. A pathologist's road map to benign, precancerous, and malignant intraepithelial proliferations in the fallopian tube. *Adv Anat Pathol*. 2010;17(5):293–302.
59. Karst AM, Drapkin R. Ovarian cancer pathogenesis: a model in evolution. *J Oncol*. 2010;2010:932371.
60. Esselen KM, Rodriguez N, Growdon W, Krasner C, Horowitz NS, Campos S. Patterns of recurrence in advanced epithelial ovarian, fallopian tube and peritoneal cancers treated with intraperitoneal chemotherapy. *Gynecol Oncol*. 2012;127(1):51–54.
61. Ince TA, et al. Transformation of different human breast epithelial cell types leads to distinct tumor phenotypes. *Cancer Cell*. 2007;12(2):160–170.
62. Clauss A, et al. Overexpression of elafin in ovarian carcinoma is driven by genomic gains and activation of the nuclear factor κB pathway and is associated with poor overall survival. *Neoplasia*. 2010;12(2):161–172.
63. Tibes R, et al. Reverse phase protein array: validation of a novel proteomic technology and utility for analysis of primary leukemia specimens and hematopoietic stem cells. *Mol Cancer Ther*. 2006; 5(10):2512–2521.